

---

# Multiple ionization processes in diatomic molecules exposed to short intense laser pulses

The Monte Carlo wave packet approach

---

Henriette Astrup Leth

...

Progress report

The Lundbeck Foundation Theoretical Center  
for Quantum System Research  
Department of Physics and Astronomy  
Aarhus University  
May 22, 2009.





---

# Contents

<b>Preface</b>	<b>iii</b>
Notation . . . . .	iii
Acknowledgements . . . . .	iii
<b>1 Introduction</b>	<b>1</b>
<b>2 Diatomic molecules in laser fields</b>	<b>3</b>
2.1 Coulomb explosion . . . . .	3
2.1.1 Experimental setup . . . . .	3
2.2 The Hamiltonian operator . . . . .	4
2.3 Theoretical proposals . . . . .	6
<b>3 The Monte Carlo wave packet technique</b>	<b>7</b>
3.1 The general principles . . . . .	7
3.2 Decay in a two-level system . . . . .	8
3.3 Equivalence to the master equation . . . . .	10
<b>4 Double ionization of H<sub>2</sub></b>	<b>11</b>
4.1 Division into separate Hilbert spaces . . . . .	11
4.2 The Hermitian part of the Hamiltonian . . . . .	12
4.2.1 Electronic basis functions . . . . .	13
4.2.2 The Schrödinger equation . . . . .	13
4.2.3 The electronic potentials . . . . .	14
4.2.4 Electron coupling to the field . . . . .	14
4.2.5 Nuclear kinetic energy . . . . .	15
4.3 The total Hamiltonian . . . . .	16
4.3.1 The ionization rates . . . . .	17
4.4 Calculation strategy . . . . .	17
<b>5 Computational remarks</b>	<b>20</b>
5.1 Propagating the wave function . . . . .	20

## Contents

5.1.1	Finite difference grid representation . . . . .	21
5.2	Reducing the computational effort . . . . .	21
5.2.1	Simplifications in the two-level case . . . . .	22
5.2.2	Simplifications in the case of H <sub>2</sub> . . . . .	23
<b>6</b>	<b>Results</b>	<b>25</b>
6.1	Nuclear dynamics of the neutral molecule . . . . .	25
6.2	Dynamics in the singly ionized molecule . . . . .	26
6.2.1	The second jump . . . . .	26
6.2.2	Jump probabilities . . . . .	27
6.3	Comparison with experiments . . . . .	28
6.4	Using other pulse parameters . . . . .	29
<b>7</b>	<b>Conclusion</b>	<b>30</b>
7.1	Outlook . . . . .	30
	<b>Bibliography</b>	<b>32</b>



---

# Preface

This progress report contains a summary of the work I have done during the first years of my Ph.D. studies at the Lundbeck Foundation Theoretical Center for Quantum System Research, Department of Physics and Astronomy, Aarhus University.

The work centers around ionization processes in molecules exposed to short intense laser pulses, i.e. pulses in the femtosecond regime and with intensities on the order of  $10^{14}$  W/cm<sup>2</sup>. Initial calculations on the ionization of H<sub>2</sub><sup>+</sup> were made using the strong field approximation in a static two-state model. This work resulted in the publication of Ref. [1] but will only be very briefly described in this report. Instead, the main focus will be on our recent work concerning nuclear dynamics in double ionization of H<sub>2</sub> using the Monte Carlo wave packet technique. Results have at the present time been submitted for publication [2].

## Notation

Atomic units are used throughout this report unless stated otherwise. This means that the mass of the electron  $m_e$ , the absolute value of the charge of the electron  $|e|$ , the reduced Planck's constant  $\hbar$  and the Bohr radius  $a_0$  all equal unity.

## Acknowledgements

I would like to thank my supervisor Lars Bojer Madsen for great guidance throughout my studies and Klaus Mølmer for useful insights into the Monte Carlo wave packet technique.

Henriette Astrup Leth, May 2009



---

# Introduction

The interplay of matter and electromagnetic radiation have been studied for centuries. However, due to the continuing development of new light sources, the theoretical description of the interaction is still far from complete. Gaining as much information about different phenomena as possible is an important task. Both because it pleases the curious mind but also because the knowledge obtained may facilitate development of new materials, devices or techniques that are useful to all of us on a daily basis.

Going back in history, the first major step in the theoretical understanding of light-matter interaction came in 1905 when Einstein proposed the existence of the photon. The photoelectric effect adequately described the ionization of matter as transitions from discrete levels to the continuum. Formally justified by lowest order of perturbation theory and Fermi's golden rule, the law strictly concerns the absorption of one photon.

Multiphoton transitions were, however, predicted to occur at higher intensities already in 1931 by Göppert-Mayer [3] and Einstein's model was no longer sufficient. With the invention of the laser in 1960, the first multiphoton transitions were experimentally demonstrated by Kaiser and Garret using two-photon absorption in a crystal [4]. Later, also multiphoton ionization became a reality when Hall, Rabison and Branscomb used ruby lasers to induce two-photon detachment from negative halogen ions [5]. All these processes are explainable by higher orders of perturbation theory.

The intensities produced in the laboratories, however, have continued to grow. Using pulsed lasers, a large amount of energy can be released in a very short amount of time and in 1979 Agostini et al. ionized xenon atoms using pulses of  $4 \cdot 10^{13}$  W/cm<sup>2</sup> intensity [6]. Measuring the energy of the photoelectron produced, they were the first to observe above-threshold ionization, where the electron absorbs more photons than required to ionize. Reaching this intensity regime, perturbation theory breaks down and the laser no longer just couples states, it also modifies them noticeably. This complicates the theoretical description significantly but also enables new phenomena to appear. The modification of the state depends on both intensity, pulse shape and wave length and it is hence possible to optimize the interaction towards a certain goal. This goal may be breaking of a polyatomic molecule at a specific point or efficient excitation of states normally unavailable because of selection rules. Another possibility is to use the coherent excitation of highly energetic continuum states obtained in above-threshold ionization to generate extremely

high harmonics. This was suggested by Shore and Knight in 1987 [7] and has led to the later production of attosecond pulses.

Using pulsed lasers not only allows for high intensity processes to appear, it also introduces a time limit in the interaction. With durations down to 10 fs, the regime of nuclear motion is reached and pump-probe experiments have in the last decade allowed for real time studies of molecular kinetics [8–10]. In such experiments, an initial pulse suddenly initiates a dissociation process, while another second pulse ionizes the molecule. This reveals the present nuclear wave function by examining the kinetic energy distribution of the outgoing nuclei. Besides obtaining information about physical processes, femtosecond pulses and their interaction with matter are nowadays widely used by the industry for everything from precision processing of materials to eye surgery due to the low heat dispersion compared to continuous wave lasers.

It is hoped that understanding light-matter interaction of short intense laser pulses better than it is the case today will lead to several further applications. One major goal is control over chemical processes. Using femtosecond and attosecond pulses in combination, experiments on ionization and dissociation of  $D_2$  has already shown the ability to selectively place the remaining electron on one of the outgoing fragments [11]. When extended to other molecules, this control may give rise to production of new materials or reduction in unwanted byproducts of industrial processing.

However, the theoretical methods needed in order for full chemical control to be a reality are still far from being well established. With field strengths comparable to the Coulomb field within the molecules and pulse durations on the same timescale as nuclear motion, no usual approaches apply. It is therefore of high importance to investigate relatively simple physical processes in short intense laser fields in order to get one step closer at the time. Seen individually, each step might look rather unimportant but placed in the right context this is indeed not the case. For further reviews on the current state of theory in this field see Refs. [12–15].

This progress report centers around strong field ionization of diatomic molecules exposed femtosecond laser pulses. The main concern is on the nuclear dynamics, and the Monte Carlo wave packet (MCWP) technique is applied in order to account for both dissociation and ionization on an equal footing. Double ionization of  $H_2$  is used as example throughout the report but the model is easily extendable to other diatomic molecules as well. Chapter 2 provides a sketch of the experimental setup and a discussion of the main theoretical tasks. Some existing models are presented as well. In chapter 3 the MCWP technique is introduced and applied to a simple two-level system before it is generalized to double ionization of  $H_2$  in chapter 4. A few computational remarks are given in chapter 5 and the results are presented in chapter 6.



---

# Diatomic molecules in laser fields

In this chapter an introduction to diatomic molecules in strong laser pulses is given. First, the physical process of interest is presented. This is followed by a construction of the Hamiltonian which also shows the complexity of the problem. Some previous theoretical attempts are sketched in the end.

## 2.1 Coulomb explosion

Consider a diatomic molecule exposed to a short intense laser pulse. Short here implies durations on the timescale of the nuclear motion ( $\sim$  few femtoseconds) and intense corresponds to electric field strengths comparable to those of the Coulomb field within the molecule ( $\sim 10^{14}$  W/cm<sup>2</sup>). This mixture of competing forces gives a variety of possibilities for the evolution of the molecule. To mention some the molecule may ionize, dissociate or both ionize and dissociate. Alternatively, the electrons may backscatter from the ionization leading to additional ionization or reabsorption under emission of high harmonic generation.

The process of concern in this report is Coulomb explosion. Coulomb explosion represents the possibility where one or several electrons are removed leaving the two nuclear centers charged, resulting in fast dissociation due to the electrostatic repulsion. Both electrons and positive ions leave the interaction region and may be detected, however, in this report the latter particles are of main concern. Experimental determination of the kinetic energy distribution of the ions gives information about the dissociation process. As a consequence the theoretical model presented later will aim to reproduce this distribution.

### 2.1.1 Experimental setup

To measure the kinetic energy distribution from Coulomb explosion, a COLTRIMS (cold target recoil ion momentum spectroscopy) setup similar to the one sketched in Fig. 2.1 is often used [16, 17]. The COLTRIMS technique allows for simultaneous detection of both electrons and ions. A gas jet of cold molecules ( $\sim 10$  K) is created in a supersonic expansion of precooled molecules ( $\sim 50$  K) and sent through the focus of an ionizing laser. The motion of the particles is slow on the timescale of the pulse duration and they will

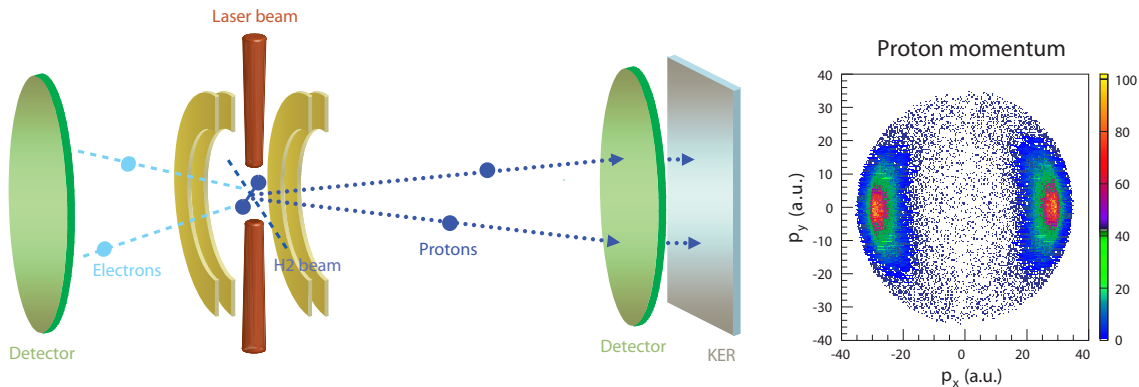


**Figure 2.1** | Sketch of the COLTRIMS setup in the case of double ionization of  $\text{H}_2$ . A beam of neutral molecules is sent through a laser focus and electric and magnetic fields guide the charged fragments towards two detectors. The positions on the detectors and the times of impact allows for recreation of the momentum vectors.

seem stationary during the experiment. The orientation is isotropic. Constant electric and magnetic fields guide the ions and electrons toward two channel plate detectors after the ionization. From the measured time-of-flight of the particles and their position of impact on the detectors, the three-dimensional momentum vector can be obtained from simple classical calculations. By integrating over angles, the total kinetic energy release (KER) is determined.

## 2.2 The Hamiltonian operator

In order to describe Coulomb explosion of diatomic molecules theoretically, the Hamiltonian operator of the system is needed. The cold target is sufficiently dilute to neglect the interaction among the individual molecules and the field is sufficiently intense to be treated classically. Considering a molecule with  $N$  electrons, as sketched in Fig. 2.2 for the case of  $N = 1$ , the first step is to write up the Lagrangian function

$$L = T - U + L_{nc}. \quad (2.1)$$

The kinetic energy  $T$  and the conservative part of the potential energy  $U$  are easily determined, while the non-conservative part  $L_{nc}$  is found by rearrangement of the Lagrange equations to resemble the classical equations of motion. The generalized coordinates  $q_i$  are in this case the  $x$ ,  $y$  and  $z$  coordinates of the particles, while the generalized momenta turns out not to equal  $m_j v_{x_j}$  but rather

$$p_{x_j} = \frac{\partial}{\partial v_{x_j}} L = m_j v_{x_j} - Z_j A_x(\vec{r}_j) \quad (2.2)$$

for the  $x$  component of particle  $j$  and similarly for the other components. Definitions of the symbols are given in Fig. 2.2.

The Hamiltonian function is now obtained using

$$H \equiv \sum_{i=1}^{3(N+2)} p_i \dot{q}_i - L. \quad (2.3)$$

$m_x$ : mass of particle $x$ $v_x$ : velocity of particle $x$ $Z_x$ : charge of particle $x$ $\phi(\vec{r})$ : scalar potential in $\vec{r}$ $\vec{A}(\vec{r})$ : vector potential in $\vec{r}$
$\vec{P}_c = -i\nabla_{\vec{R}_c}$ $\vec{P}_{AB} = -i\nabla_{\vec{R}_{AB}}$ $\vec{p}_j = -i\nabla_{\vec{q}_j}$ $M = m_A + m_B + N$ $\mu = m_A m_B / (m_A + m_B)$

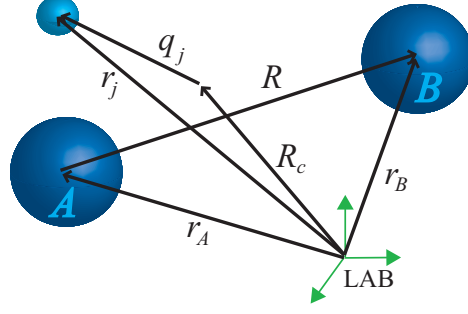


**Figure 2.2** | Definition of the symbols used in the text. The diatomic molecule is sketched in the case of  $N = 1$  and position vectors are given in a laboratory fixed coordinate system.

However, before writing out the final result, some simplifications can be made in order to reduce the complexity. Since the spatial variation of the external field on the length scale of the molecule is negligible, the dipole approximation is employed and the vector field is only evaluated at the position of the center of mass. The terms including the scalar potential are eliminated by a gauge transformation to the Coulomb gauge, in which the scalar potential is zero and the generalized momenta and the vector field commute giving the following result [18]:

$$\begin{aligned}
 H = & \frac{1}{2M} \vec{P}_c^2 + \frac{1}{2\mu} \vec{P}_{AB}^2 + \sum_{j=1}^N \vec{p}_j^2 - \frac{1}{2M} \sum_{j,j'=1}^N \vec{p}_j \vec{p}_{j'} + \frac{1}{2} \left( \frac{Z_A^2}{m_A} + \frac{Z_B^2}{m_B} + N \right) \vec{A}(\vec{R}_c)^2 \\
 & - \frac{1}{M} (Z_A + Z_B - N) \vec{P}_c \vec{A}(\vec{R}_c) + \frac{1}{M} \sum_{j=1}^N (Z_A + Z_B - N) \vec{p}_j \vec{A}(\vec{R}_c) - \left( \frac{Z_A}{m_A} - \frac{Z_B}{m_B} \right) \vec{P}_{AB} \vec{A}(\vec{R}_c) \\
 & + \sum_{j=1}^N \vec{p}_j \vec{A}(\vec{R}_c) + \frac{Z_A Z_B}{|\vec{r}_A - \vec{r}_B|} - \sum_{j=1}^N \frac{Z_A}{|\vec{r}_j - \vec{r}_A|} - \sum_{j=1}^N \frac{Z_B}{|\vec{r}_j - \vec{r}_B|} + \sum_{j < j'} \frac{1}{|\vec{r}_j - \vec{r}_{j'}|}. \quad (2.4)
 \end{aligned}$$

The kinetic energy is here responsible for the first four terms. The motion of the center of mass is often neglected (term 1) and so is the cross terms in the electronic momenta (term 4) since these are down by a factor of  $M$  compared to the diagonal terms (term 3). The energy shift due to the external field (term 5) can be eliminated by a trivial phase transformation but is here kept since a later gauge transformation to the velocity gauge will produce a similar term with opposite sign. Coupling to the external field is responsible for the next four terms. Once again, by neglecting the center of mass motion (term 6) and eliminating terms down by a factor of  $M$  (term 7) the problem simplifies. For homonuclear molecules term 8 vanishes and the electronic coupling is the only one remaining (term 9). The last four terms concern electrostatic interactions.

By applying all of the above approximations, the Hamiltonian operator simplifies. However, the corresponding Schrödinger equation is still extremely complicated to solve. Even in the two electron case of  $\text{H}_2$ , used as an example in this report, the full problem is at present day impossible to handle by ab initio calculations. The high intensity of the laser field introduces a very strong coupling and usual approaches based on perturbation theory are all useless. Extensive further theoretical work and new approximation methods are hence of high importance in order to predict the outcome of experiments.

## 2.3 Theoretical proposals

In recent years, several attempts to describe the KER of Coulomb explosion have been made. Unfortunately, the presented models have all relied on ad hoc input and fitting parameters or been unextendable to systems of more than one electron.

In the one-electron case of  $\text{H}_2^+$  it is possible to make beyond Born-Oppenheimer grid calculations using all three coordinates for the electron and the internuclear separation simultaneously [19, 20]. However, in order to extend this to  $\text{H}_2$ , the first ionization needs to be accounted for in a very ad hoc manner. In Ref. [20] this is done by suddenly turning on the laser field two cycles before the peak of the pulse and using the vibrational ground state of  $\text{H}_2$  as the initial condition in  $\text{H}_2^+$ . Despite this critical approximation, the agreement with experiments is very good. It is, however, at present day impossible to extend this model to larger molecules and also the physical insight gained is limited.

Some simpler models have been proposed in an attempt to predict the outcome in a way extendable to larger systems. Using the Born-Oppenheimer approximation and including only the two lowest lying electronic states in  $\text{H}_2^+$ , reproduction of the KER spectrum is possible for some pulse parameters [21, 22]. In the model interference between the net two-photon transition between the  $1s\sigma_g$  and  $2p\sigma_u$  state generate localized electrons which subsequently ionize causing peaks in the theoretical spectrum also observed in the experimental one. The initial creation of  $\text{H}_2^+$  is once again included using an artificial pulse envelope and the initial wave function is mapped directly from the ground state of  $\text{H}_2$ . No theoretical model have so far been able to treat both ionizations on an equal footing.

One way to get around the problem of describing multiple ionizations is to study  $\text{H}_2^+$  directly [23, 24]. Some experimental data are in this case reproduced by examining crossings of Born-Oppenheimer curves [23]. Using the  $1s\sigma_g$ ,  $2p\sigma_u$  and  $1/R$  potential curve and shifting these by some integer number of photon energies, ionization is more likely to happen at the resulting crossings. The internuclear separations at the crossings correspond to potential energies of  $1/R$  and by adding a typical kinetic energy, the locations of the peaks in the resulting spectrum are predicted. However, this method cannot predict the weight of the individual peaks and experimental data are mimicked by a fit of Gaussian functions.

The final theoretical attempt to be mentioned here, is to assume that the nuclei are fixed during the pulse. This approximation was used in the very first period of my Ph.D. studies and applies when the pulse duration is no longer than 25 fs in the case of  $\text{H}_2^+$  [1]. Using the strong field approximation, a two state model including the field free molecule as initial state and a completely separated nuclei and electron as final state, good agreement with experiments [9, 25] is obtained. However, for longer pulse durations, the model breaks down and it cannot be used to treat several ionizations.

By giving these examples, I hope to have convinced the reader that studying multiple ionization processes in short intense laser pulses is extremely complicated. At present day, only very limited theoretical proposals are published. The purpose of this report is to present a simple model which describes nuclear dynamics as well as multiple ionizations on an equal footing. The MCWP technique takes advantage of already available potential surfaces, dipole moment functions and electronic ionization rates and is in this way capable of predicting the outcome of experiments without any ad hoc inputs. In addition, this is done in a computationally very efficient way easily extendable to larger systems.

---

## The Monte Carlo wave packet technique

Before a detailed description of multiple ionization processes in diatomic molecules using the MCWP technique can be given, this chapter introduces the main concepts of the technique. After some general remarks, a simple example of decay in a two-level system is presented and the validity of the method is discussed.

### 3.1 The general principles

In order to describe the statistical state of a quantum system, the density matrix is often used. The density matrix is the quantum-mechanical analogue to a phase-space density in classical statistical mechanics and is useful when describing ensembles of particles. However, in order to find the density matrix, one has to solve the master equation for all  $N^2$  entrances, where  $N$  is the number of states. This should be compared to  $N$  in the case of solving the Schrödinger equation. Motivated by this, the MCWP approach was introduced in the early nineties [26–28] and allows for wave function based solutions of the master equation.

Consider a quantum system for which the complete Hamiltonian is not known, i.e. some couplings are only described in the form of the transition rates they induce. This may for instance be the case when coupling to the surroundings transfers population to and from the system but also in cases where the internal coupling is unknown or too complex to be included. In order to account for this coupling in a wave function picture and not using density matrices, several questions comes to mind. First of all, how to account for the break of reversibility normally incorporated in the Schrödinger equation, which can simply not be maintained when losses or gains are included. The solution comes in the form of gedanken experiments. In each time step of the quantum state evolution a measurement is performed giving information about the system and hence maybe altering it. In the case of ionization of an atom, this may be in the form of an imaginary electron detector placed near by, forcing the system to be ionized if an electron is detected. In order for this approach to work, it is of course important that the detection take place sufficiently far away from the ion, that it does not directly alter the evolution of the system.

To quantify this approach of using gedanken experiments, a Hamiltonian operator is

introduced on the form

$$H = H_s - \frac{i}{2} \sum_m C_m^\dagger C_m, \quad (3.1)$$

where  $H_s$  is the Hamiltonian without the transition terms and  $C_m$  is a transition operator transferring the system from an initial state  $|i\rangle$  to a final state  $|f\rangle$  with rate  $\Gamma_m$

$$C_m = \sqrt{\Gamma_m} |f\rangle \langle i|. \quad (3.2)$$

Due to the imaginary correction to the Hamiltonian, the operator is no longer Hermitian and hence it does not conserve the norm of the wave function when this is propagated in time. It is this drop in norm which is responsible for whether a transition occurs or not. In each time step, a random number between zero and unity is chosen and if it is found to be smaller than the drop in norm this corresponds to a click in the imaginary detector and hence a transition. A quantum jump is then applied in the form of the jump operator. If on the other hand the random number is larger than the drop in norm, it corresponds to a null detection and no transition occurs. The wave function is in this case renormalized. In order to obtain the correct physical evolution of an ensemble of atoms, many different realizations are performed and the results are averaged.

## 3.2 Decay in a two-level system

Before discussing the validity of the MCWP technique, a simple example is here given in order to provide a better overview of the method.

Consider the system sketched in Fig. 3.1 with ground state  $|g\rangle$ , excited state  $|e\rangle$  and a rate of decay  $\Gamma$ . The transition operator equals

$$C_1 = \sqrt{\Gamma} |g\rangle \langle e|, \quad (3.3)$$

making the non-Hermitian Hamiltonian operator take the form

$$\begin{aligned} H &= H_s - \frac{i}{2} \sum_m C_m^\dagger C_m \\ &= 0 \cdot |g\rangle \langle g| + E \cdot |e\rangle \langle e| - \frac{i}{2} \sqrt{\Gamma} |e\rangle \langle g| \sqrt{\Gamma} |g\rangle \langle e| \\ &= E |e\rangle \langle e| - \frac{i}{2} \Gamma |e\rangle \langle e|. \end{aligned} \quad (3.4)$$

Starting in the state  $|\phi_0\rangle = \alpha_0 |g\rangle + \beta_0 |e\rangle$  at time  $t = 0$ , the state of the system at a later time  $t = dt$  can be found by applying the time evolution operator

$$U(dt, 0) = \exp(-iHdt) \approx 1 - iHdt. \quad (3.5)$$

One obtains

$$\begin{aligned} |\tilde{\phi}_{dt}\rangle &= U(dt, 0) [\alpha_0 |g\rangle + \beta_0 |e\rangle] \\ &= \left( 1 - iE |e\rangle \langle e| dt - \frac{1}{2} \Gamma |e\rangle \langle e| dt \right) [\alpha_0 |g\rangle + \beta_0 |e\rangle] \\ &= \alpha_0 |g\rangle + \beta_0 |e\rangle - iE \beta_0 dt |e\rangle - \frac{1}{2} \Gamma \beta_0 dt |e\rangle \end{aligned} \quad (3.6)$$

### Decay in a two-level system

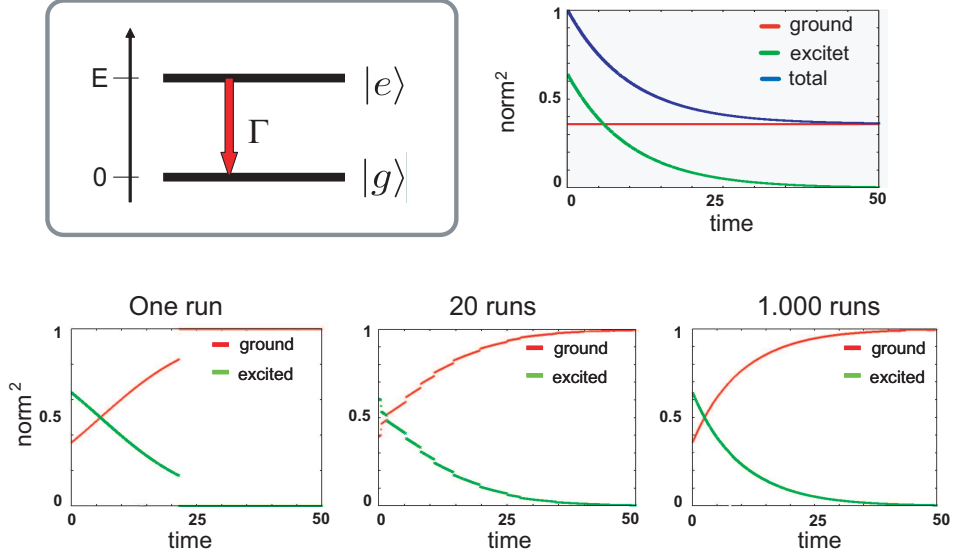


**Figure 3.1** | Decay in a two level system with  $\alpha_0 = 0.6$ ,  $\beta_0 = 0.8$ ,  $\Gamma = 0.1$  and  $E = 0.0001$ . The top right figure gives the evolution if propagating using the non-Hermitian Hamiltonian and doing no renormalization. Bottom shows the MCWP results for different numbers of runs.

and

$$\begin{aligned} \langle \tilde{\phi}_{dt} | \tilde{\phi}_{dt} \rangle &= |\alpha_0|^2 + |\beta_0|^2 + \frac{1}{4}\Gamma^2|\beta_0|^2 dt^2 - \Gamma|\beta_0|^2 dt + E^2|\beta_0|^2 dt^2 \\ &\approx 1 - \Gamma|\beta_0|^2 dt = 1 - dp \end{aligned} \quad (3.7)$$

Here terms of order  $dt^2$  are neglected and the initial state is assumed to be normalized. The tilde indicates that the norm is no longer unity. Next, a draw of a random number  $\epsilon$  between zero and one will determine the evolution.

If  $\epsilon > dp$  no jump occurs and a renormalization is performed. By examining Eq. (3.6), it is seen that the population in  $|g\rangle$  still equals  $|\alpha_0|^2$ , while the population in  $|e\rangle$  has dropped by  $\Gamma dt |\beta_0|^2$  thus altering the relative population among the two when renormalizing. This implies that population is transferred from the excited state to the ground state even if no jump is applied. This may seem strange, but is due to the fact that a null detection signal in the imaginary detector (like a positive one) gives information about the system and hence may alter it.

If  $\epsilon < dp$  a jump occurs and the jump operator is applied to the initial state,

$$|\tilde{\phi}_{dt, jump}\rangle = C_1 |\phi_0\rangle = \sqrt{\Gamma} |g\rangle \langle e | \phi_0\rangle = \text{const} \cdot |g\rangle, \quad (3.8)$$

which after a renormalization gives

$$|\phi_{dt}\rangle = |g\rangle. \quad (3.9)$$

Fig. 3.1 shows the averaged results for 1 run, 20 runs and 1000 runs for the case  $\alpha_0 = 0.6$ ,  $\beta_0 = 0.8$ ,  $\Gamma = 0.1$  and  $E = 0.0001$ . Consider the case of only one run. In the first 21 units of time no jump occurs and population is transferred from the excited state to the ground state. The amount of transfer is too small to result in the correct half time of  $\ln(2)/\Gamma = 6.9$  and the correct evolution is only obtained when averaging over many different realizations including jumps. This is seen from the figure in the case of 1000 runs.

### 3.3 Equivalence to the master equation

As shown above, the MCWP technique succeeds in predicting the evolution of a two-level system with decay, and this without any knowledge about the coupling between the two states besides the transition rate. This problem may also be solved using the master equation and the MCWP method works because the two approaches are in fact equivalent. To see this, consider the two operators

$$\sigma_0 = |\phi_0\rangle\langle\phi_0| \quad \sigma_{dt} = |\phi_{dt}\rangle\langle\phi_{dt}|. \quad (3.10)$$

The average value of the latter operator equals the density operator  $\rho_s$  of the system at the time  $dt$  and it may be determined by knowing that the system with probability  $(1 - dp)$  is in the renormalized state  $|\tilde{\phi}_{dt}\rangle/\sqrt{1 - dp}$  and with probability  $dp$  in the jumped state  $C_1|\phi_0\rangle/\sqrt{dp/dt}$ . By neglecting terms of order  $dt^2$ , it is seen that [29]

$$\begin{aligned} \bar{\sigma}_{dt} &= (1 - dp) \cdot \frac{|\tilde{\phi}_{dt}\rangle\langle\tilde{\phi}_{dt}|}{1 - dp} + dp \cdot \frac{C_1|\phi_0\rangle\langle\phi_0|C_1^\dagger}{dp/dt} \\ &= |\tilde{\phi}_{dt}\rangle\langle\tilde{\phi}_{dt}| + dtC_1|\phi_0\rangle\langle\phi_0|C_1^\dagger \\ &= (1 - iH_s dt - C_1^\dagger C_1 dt)|\phi_0\rangle\langle\phi_0|(1 + iH_s dt - C_1^\dagger C_1 dt) + dtC_1|\phi_0\rangle\langle\phi_0|C_1^\dagger \\ &= \sigma_0 + idt\sigma_0 H_s - idtH_s \sigma_0 - dt\sigma_0 C_1^\dagger C_1 - dtC_1^\dagger C_1 \sigma_0 + dtC_1 \sigma_0 C_1^\dagger \\ &= \sigma_0 + idt[\sigma_0, H_s] + dt\mathfrak{L}(\sigma_0), \end{aligned} \quad (3.11)$$

where  $\mathfrak{L}$  is the relaxation superoperator introduced in density matrix theory and defined as

$$\mathfrak{L}(\rho_s) = - \left[ \sum_m C_m^\dagger C_m \rho_s + C_m^\dagger C_m \rho_s \right] + \sum_m C_m \rho_s C_m^\dagger. \quad (3.12)$$

Averaging over different values of  $\sigma_0$  and using  $(\bar{\sigma}_{dt} - \bar{\sigma}_0)/dt \approx d/dt \bar{\sigma}_0$  for small  $dt$ , the master equation can be recovered,

$$\frac{d\bar{\sigma}_0}{dt} = i[\bar{\sigma}_0, H_s] + \mathfrak{L}(\bar{\sigma}_0). \quad (3.13)$$

Accordingly, the two methods are equally correct.



---

## Double ionization of H<sub>2</sub>

Having introduced the MCWP technique, it is now time to apply the technique to double ionization of H<sub>2</sub> in short intense laser pulses. This is done by first dividing the problem into three different Hilbert spaces that can all be treated by the MCWP approach. The transitions among each space are described in terms of rates and can hence be viewed in the context of a system with gains and losses of population. The Hermitian part of the Hamiltonian operator is deduced, with a detailed discussion of each term and later is the non-Hermitian jump terms added as well. An overview over the calculation strategy is given in the end.

### 4.1 Division into separate Hilbert spaces

The electron is much lighter than the proton and hence moves on a different timescale. This justifies the Born-Oppenheimer approximation, in which the electronic motion is determined for fixed nuclei leading to an effective potential used in the subsequent determination of the nuclear dynamics. In the case of double ionization of H<sub>2</sub>, many different electronic states are involved. Some correspond to having two electrons bound, while one or both of the electrons in others are in continuum states. In order to significantly simplify the calculations, a division into three Hilbert spaces is made, each one neglecting the electrons infinitely far from the nuclei. The first space contains four particles (H<sub>2</sub>), the second three particles (H<sub>2</sub><sup>+</sup>) and the last only the two protons (H<sub>2</sub><sup>++</sup>). This simplifies the Hamiltonian but hinders the usual approach of solving the Schrödinger equation which assumes a single Hilbert space. As a consequence, we now turn to the MCWP approach and consider each space with losses and gains of population to and from the other spaces.

In order to apply the MCWP technique to each of the Hilbert spaces, it is important that the emitted electron does not return to the parent ion. Otherwise a gedanken measurement will directly alter the evolution of the system which must not happen. This is ensured by the broad continuum of final states. The different final state components will accumulate sufficient phase differences during the ionization process that the quantum state population does not coherently return to the initial state, unlike Rabi oscillations between discrete levels. It should be noted, however, that the field ionization may in many situations cause transient oscillations between the population of the ionized and the

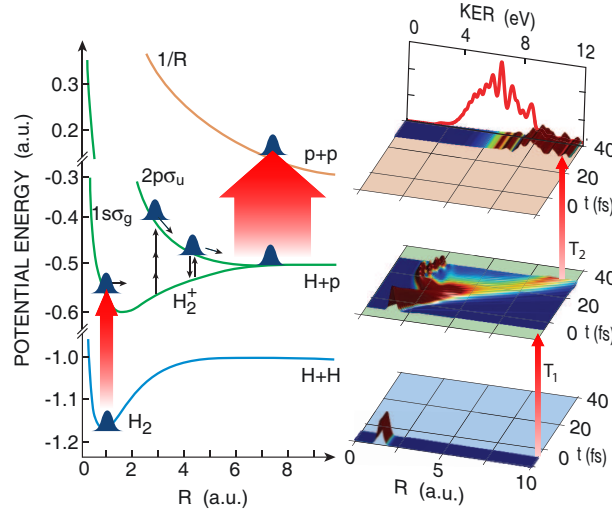


**Figure 4.1** | Sketch of the three Hilbert spaces included to describe double ionization of H<sub>2</sub>. The left panel shows the Born-Oppenheimer potential curves, while the right panel shows how the nuclear wave packet is transferred from one space to the other in instantaneous jumps. In the double ionized Hilbert space, the KER distribution, can be determined.

initial state [30, 31]. Since the ionization probability is small in the present case, these oscillations are assumed to be insignificant and we neglect recapture and now turn to using the MCWP technique on double ionization of H<sub>2</sub>.

An overview of the model is sketched in Fig. 4.1. Starting in the H<sub>2</sub> space, only one electronic state is included, namely the ground state  $(1s\sigma_g)^2$ . The system is propagated in the ground state until an electron is detected at time  $T_1$ . The nuclear wave function is now instantaneously transferred to the H<sub>2</sub><sup>+</sup> space. For the singly ionized molecule we include two electronic states; the bonding  $1s\sigma_g$  state and the dissociative  $2p\sigma_u$  state. After some time with null detection and nuclear dynamics in these coupled states an electron is detected at time  $T_2$  and the system is transferred to the final Hilbert space. Here only two protons are present and the absence of electrons leads to an effective  $1/R$  potential due to the nuclear repulsion.

Averaging the outcome of different simulations gives the total evolution of the system.

## 4.2 The Hermitian part of the Hamiltonian

In order to write up the Hamiltonian operator, Eq. (2.4) is used. We need the operator for both H<sub>2</sub>, H<sub>2</sub><sup>+</sup> and H<sub>2</sub><sup>++</sup>, however, in the following we focus only on H<sub>2</sub> which gives them all as special cases. Applying the approximations discussed in chapter 2 and using  $N = 2$  one obtains

$$\begin{aligned}
 H_s = & \frac{1}{2\mu} \vec{P}_{AB}^2 + \sum_{j=1,2} \frac{1}{2} \vec{p}_j^2 + \sum_{j=1,2} \vec{p}_j \cdot \vec{A}(\vec{R}_c) + \frac{1}{2} N \vec{A}(\vec{R}_c)^2 \\
 & + \frac{Z_A Z_B}{|\vec{r}_A - \vec{r}_B|} - \sum_{j=1,2} \frac{Z_A}{|\vec{r}_j - \vec{r}_A|} - \sum_{j=1,2} \frac{Z_B}{|\vec{r}_j - \vec{r}_B|} + \frac{1}{|\vec{r}_1 - \vec{r}_2|}. \quad (4.1)
 \end{aligned}$$

Here the coupling to the external field is included, even though we are not interested in the terms responsible for jumps among the different Hilbert spaces. The coupling, however,

affects the evolution in the individual spaces as well and needs to be taken into account. In Eq. (4.1) the coupling takes the form  $\vec{\rho}_j \cdot \vec{A}$ , often referred to as the velocity gauge. A simple gauge transformation can, however, alter the appearance of the coupling term to the length gauge,

$$\sum_{j=1,2} \vec{\rho}_j \cdot \vec{A}(\vec{R}_c) + \frac{1}{2} N \vec{A}(\vec{R}_c)^2 \rightarrow \sum_{j=1,2} \vec{q}_j \cdot \vec{E}(\vec{R}_c). \quad (4.2)$$

This is done as usual by using  $H_l = T H_v T^\dagger + i \frac{dT}{dt} T^\dagger$  where the subscripts  $l$  and  $v$  denotes length and velocity gauge respectively and  $T$  is the operator

$$T = \exp(i \sum_{j=1,2} \vec{\rho}_j \cdot \vec{A}(\vec{R}_c)). \quad (4.3)$$

A change of gauge does not change the outcome of exact calculations but when applying approximations this is no longer the case. The length gauge is chosen here since it probes mainly large distances which is favorable in the case of ionization processes.

For simplification of the later discussion, the first term in the Hamiltonian, Eq. (4.1), is denoted  $T_{nuc}$ , the terms involving the external field  $L_{elec}$ , and the rest are collected under the symbol  $H_{elec}$ ,

$$H_s = T_{nuc} + L_{elec} + H_{elec}. \quad (4.4)$$

The next step is to express these individual terms in a basis of electronic eigenstates.

### 4.2.1 Electronic basis functions

As discussed in the last section we adapt the Born-Oppenheimer approximation and study the nuclear evolution in a basis of electronic solutions. These are the states  $|\phi_{Ra}\rangle$  fulfilling

$$H_{elec}(R) |\phi_{Ra}\rangle = E_a(R) |\phi_{Ra}\rangle. \quad (4.5)$$

The solutions depend on both the energy  $E_a$  for the electronic state  $a$  and the internuclear separation  $R$ . Even though there are infinitely many electronic states, we, as discussed above, only include four. These are  $(1s\sigma_g)^2$  in  $H_2$ ,  $1s\sigma_g$  and  $2p\sigma_u$  in  $H_2^+$ , and the doubly ionized state  $H_2^{++}$ , for short denoted  $h$ ,  $g$ ,  $c$  and  $u$ . The states are orthonormal in  $a$  and we assume them to span a complete basis. Though many more states could be included, the four discussed here show to be sufficient to reproduce the physical picture quite well.

The total state ket  $|\Psi\rangle$  can now be expressed in the basis of electronic solutions

$$|\Psi\rangle = \sum_a \int d\vec{R} X_a(\vec{R}, t) |\phi_{Ra}\rangle \otimes |\vec{R}\rangle, \quad (4.6)$$

where the prefactors  $X_a(\vec{R}, t)$  are the nuclear wave functions and  $|\vec{R}\rangle$  the position eigenkets of the nuclear coordinate.

### 4.2.2 The Schrödinger equation

In order to express the Hamiltonian operator in the chosen basis, we turn to the time-dependent Schrödinger equation,

$$H_s |\Psi\rangle = i \frac{d}{dt} |\Psi\rangle. \quad (4.7)$$

Inserting Eq. (4.6), projecting on both sides with  $\langle R' | \otimes \langle \phi_{R'a'} |$  and using that the Hamiltonian is local in space, we obtain

$$\sum_a \int d\vec{R} \delta(\vec{R}' - \vec{R}) \langle \phi_{R'a'} | H_s X_a(\vec{R}, t) | \phi_{Ra} \rangle = i \frac{d}{dt} X_{a'}(\vec{R}', t). \quad (4.8)$$

The matrix element on the left-hand side contains three terms

$$\langle \phi_{R'a'} | H_s X_a(\vec{R}, t) | \phi_{Ra} \rangle = \langle \phi_{R'a'} | [H_{elec} + L_{elec} + T_{nuc}] X_a(\vec{R}, t) | \phi_{Ra} \rangle. \quad (4.9)$$

These are discussed individually in the next three subsections.

### 4.2.3 The electronic potentials

The chosen basis states are all solutions to the electronic Hamiltonian  $H_{elec}$  and the matrix elements involving this operator are easily calculated

$$\langle \phi_{R'a'} | H_{elec} X_a(\vec{R}, t) | \phi_{Ra} \rangle = \delta_{a'a} X_a(\vec{R}, t) E_a(R). \quad (4.10)$$

The effective potentials  $E_a(R)$  are approximated using the Morse like potentials reported in Ref. [32] in the  $h$  case and in Ref. [33] in the  $g$  and  $u$  cases,

$$E_h(R) = 0.1819 \left[ e^{-2.01(R-1.4)} - 2.00e^{-1.01(R-1.4)} \right] - 1.0, \quad (4.11)$$

$$E_g(R) = 0.1025 \left[ e^{-1.44(R-2.0)} - 2.00e^{-0.72(R-2.0)} \right] - 0.5, \quad (4.12)$$

$$E_u(R) = 0.1025 \left[ e^{-1.44(R-2.0)} + 2.22e^{-0.72(R-2.0)} \right] - 0.5, \quad (4.13)$$

$$E_c(R) = \frac{1}{R}. \quad (4.14)$$

These approximations closely resemble the correct potentials as long as the internuclear distance is above 1 au.

### 4.2.4 Electron coupling to the field

In the length gauge, the coupling between an electron at position  $\vec{q}_j$  and the external field  $\vec{F}$  takes the form  $\vec{q}_j \cdot \vec{F}$ . The molecule is mainly polarizable along the internuclear axis and therefore only this component,  $q_{j,R}$ , of the dipole operator is considered. In this way, the angle  $\theta_0$  between the field polarization and the internuclear vector can be taken outside the matrix element,

$$\begin{aligned} \langle \phi_{Ra'} | L_{elec} X_a(\vec{R}, t) | \phi_{Ra} \rangle &= \sum_{j=1,2} \langle \phi_{Ra'} | (\vec{q}_{j,R} \cdot \vec{F}) X_a(\vec{R}, t) | \phi_{Ra} \rangle \\ &= |F| \cos \theta_0 \sum_{j=1,2} \langle \phi_{Ra'} | q_{j,R} | \phi_{Ra} \rangle X_a(\vec{R}, t) \end{aligned} \quad (4.15)$$

In the following, rotation of the molecule is neglected, since the characteristic timescale is on the order of 170 fs, and  $\theta_0$  is therefore a constant for each molecule [34].

Evaluation of  $\langle \phi_{Ra'} | q_{j,R} | \phi_{Ra} \rangle$  should in principle be done for all combinations of  $a$  and  $a'$ . However, since only terms in the Hamiltonian not responsible for coupling among

different Hilbert spaces are of concern, just two terms survive

$$\langle \phi_{Rg} | q_j | \phi_{Ru} \rangle = -\frac{1}{2 + 1.4R} + \frac{R}{2\sqrt{1 - p^2}} \equiv d_{gu}(R), \quad (4.16)$$

$$\langle \phi_{Ru} | q_j | \phi_{Rg} \rangle = d_{gu}(R)^* = d_{gu}(R) \quad (4.17)$$

where

$$p = (1 + R + R^2/3)e^{-R}. \quad (4.18)$$

These approximated expressions for the dipole coupling are taken from Ref. [33] and calculated using the potentials in Eqs. (4.12) and (4.13).

#### 4.2.5 Nuclear kinetic energy

Left is now only the matrix element concerning the kinetic energy of the nuclear motion. In writing out the operator, the assumption of no rotations during the pulse leads to significant simplifications,

$$\begin{aligned} T_{nuc} &= \frac{1}{2\mu} \vec{P}_{AB}^2 \\ &= -\frac{1}{2\mu} \left[ \frac{1}{R^2} \frac{\partial}{\partial R} \left( R^2 \frac{\partial}{\partial R} \right) + \frac{1}{R^2 \sin \theta} \frac{\partial}{\partial \theta} \left( \sin \theta \frac{\partial}{\partial \theta} \right) + \frac{1}{R^2 \sin^2 \theta} \frac{\partial^2}{\partial \phi^2} \right] \\ &\approx -\frac{1}{2\mu} \frac{1}{R^2} \frac{\partial}{\partial R} \left( R^2 \frac{\partial}{\partial R} \right). \end{aligned} \quad (4.19)$$

To evaluate the matrix element, the electronic eigenstates are expressed in a basis of electronic position eigenkets  $|\vec{r}\rangle$  giving the electronic wave function  $\phi_a(R, \vec{r})$

$$|\phi_{Ra}\rangle = \int d\vec{r} |\vec{r}\rangle \phi_a(R, \vec{r}). \quad (4.20)$$

Since the nuclear motion is very slow compared to the electronic motion,  $|\partial\phi_a/\partial R|$  can be neglected compared to  $|\partial X_a/\partial R|$  (the Born-Oppenheimer approximation) and one obtains

$$\begin{aligned} \langle \phi_{Ra'} | T_{nuc} X_a(\vec{R}, t) | \phi_{Ra} \rangle &= \int dr' \langle r' | \phi_{a'}^*(R, r') T_{nuc} X_a(\vec{R}, t) \int dr | r \rangle \phi_a(R, r) \\ &= \int dr' \phi_{a'}^*(R, r') \left[ -\frac{1}{2\mu} \frac{1}{R^2} \frac{\partial}{\partial R} \left( R^2 \frac{\partial}{\partial R} \right) \right] X_a(\vec{R}, t) \phi_a(R, r') \\ &= \int dr' \phi_{a'}^*(R, r') \phi_a(R, r') \left[ -\frac{1}{2\mu} \frac{1}{R^2} \frac{\partial}{\partial R} \left( R^2 \frac{\partial}{\partial R} \right) \right] X_a(\vec{R}, t) \\ &= \delta_{a'a} \left[ -\frac{1}{2\mu} \frac{1}{R^2} \frac{\partial}{\partial R} \left( R^2 \frac{\partial}{\partial R} \right) \right] X_a(\vec{R}, t). \end{aligned} \quad (4.21)$$

Since the molecule is rotationally frozen, the nuclear wave function can be expressed as

$$X_a(\vec{R}, t) = \frac{1}{R} K_a(R, t) W_a(\theta, \phi, t) \quad (4.22)$$

$$W_a(\theta, \phi, t) = \frac{1}{\sqrt{4\pi}} \delta(\theta - \theta_0) \delta(\phi - \phi_0), \quad (4.23)$$

with  $\theta_0$  and  $\phi_0$  specifying the internuclear orientation. The prefactor of  $1/R$  in the definition of the radial wave function  $K_a(R, t)$  simplifies the kinetic energy term since

$$\frac{1}{R^2} \frac{\partial}{\partial R} \left( R^2 \frac{\partial}{\partial R} \right) = \frac{1}{R} \frac{\partial^2}{\partial R^2} R, \quad (4.24)$$

leaving only  $\partial^2/\partial R^2$  in the final equation to be solved.

### 4.3 The total Hamiltonian

In order to find the total Hamiltonian, we turn to the results from the previous section. Using Eqs. (4.4) and (4.9), the Schrödinger equation equals

$$\sum_a \int d\vec{R} \delta(\vec{R}' - \vec{R}) \langle \phi_{Ra'} | (H_{elec} + L_{elec} + T_{nuc}) X_a(\vec{R}, t) | \phi_{Ra} \rangle = i \frac{d}{dt} X_{a'}(\vec{R}', t), \quad (4.25)$$

where the individual matrix elements are given in Eqs. (4.11), (4.17), and (4.25). Adding these results, using the basis set expansion of the state ket  $|\Psi\rangle$ , and inserting a few identities of the form  $1 = \sum_a \int d\vec{R} |\vec{R}\rangle \langle \vec{R}| \otimes |\phi_{Ra}\rangle \langle \phi_{Ra}| \otimes |\vec{R}\rangle \langle \vec{R}|$  leads to

$$\begin{aligned} i \frac{d}{dt} |\Psi\rangle &= \sum_a \int d\vec{R} \left[ -\frac{1}{2\mu} \frac{1}{R} \frac{\partial^2}{\partial R^2} R + E_a \right] |\phi_{Ra}\rangle \langle \phi_{Ra}| \otimes |\vec{R}\rangle \langle \vec{R}| |\Psi\rangle \\ &\quad - |F| \cos \theta_0 \int d\vec{R} d_{gu}(R) [|\phi_{Rg}\rangle \langle \phi_{Ru}| + |\phi_{Ru}\rangle \langle \phi_{Rg}|] \otimes |\vec{R}\rangle \langle \vec{R}| |\Psi\rangle. \end{aligned} \quad (4.26)$$

By comparison to the time-dependent Schrödinger equation, the Hermitian part of the Hamiltonian is seen to be

$$\begin{aligned} H_s &= \sum_a \int d\vec{R} \left[ -\frac{1}{2\mu} \frac{1}{R} \frac{\partial^2}{\partial R^2} R + E_a \right] |\phi_{Ra}\rangle \langle \phi_{Ra}| \otimes |\vec{R}\rangle \langle \vec{R}| \\ &\quad - |F| \cos \theta_0 \int d\vec{R} d_{gu}(R) [|\phi_{Rg}\rangle \langle \phi_{Ru}| + |\phi_{Ru}\rangle \langle \phi_{Rg}|] \otimes |\vec{R}\rangle \langle \vec{R}|. \end{aligned} \quad (4.27)$$

Left is only to consider the non-Hermitian part responsible for the jumps among the different Hilbert spaces. The jumps are assumed to be vertical and the three involved operators are

$$C_h = \int d\vec{R} \sqrt{\Gamma_h(\vec{R})} |\phi_{R,g}\rangle \langle \phi_{R,h}| \otimes |\vec{R}\rangle \langle \vec{R}|, \quad (4.28)$$

$$C_g = \int d\vec{R} \sqrt{\Gamma_g(\vec{R})} |\phi_{R,c}\rangle \langle \phi_{R,g}| \otimes |\vec{R}\rangle \langle \vec{R}|, \quad (4.29)$$

$$C_u = \int d\vec{R} \sqrt{\Gamma_u(\vec{R})} |\phi_{R,c}\rangle \langle \phi_{R,u}| \otimes |\vec{R}\rangle \langle \vec{R}|, \quad (4.30)$$

responsible for the transitions  $h \rightarrow g$ ,  $g \rightarrow c$  and  $u \rightarrow c$  respectively. The total Hamiltonian then reads

$$\begin{aligned} H &= H_s - \frac{i}{2} \sum_m C_m^\dagger C_m \\ &= H_s - \frac{i}{2} \sum_{a=h,g,u} \int d\vec{R} \Gamma_a(R) |\phi_{Ra}\rangle \langle \phi_{Ra}| \otimes |\vec{R}\rangle \langle \vec{R}|, \end{aligned} \quad (4.31)$$

leaving the transition rates  $\Gamma_h(R)$ ,  $\Gamma_g(R)$ , and  $\Gamma_u(R)$  as the only parameters not yet discussed.

## The ionization rates

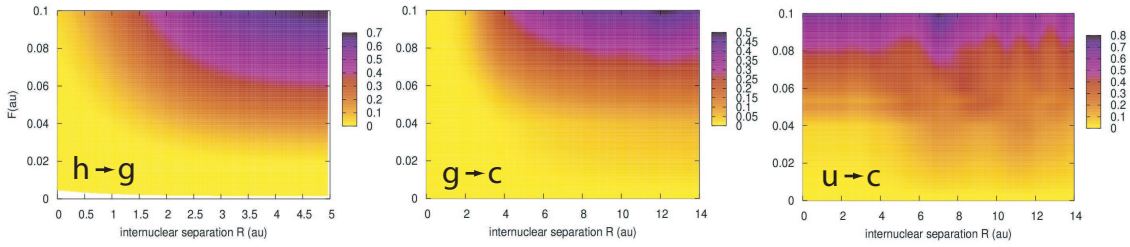


**Figure 4.2** | Ionization rates of  $\text{H}_2$  [35] and  $\text{H}_2^+$  [36] in static electric fields. The rates are plotted in atomic units to the power of 0.2 in order to gain a larger visibility of the structure.

### 4.3.1 The ionization rates

Knowing the correct ionization rates is a critical point in the MCWP approach. The rates need to be known at every instant, at every internuclear separation, and for all possible orientations of the molecule. A calculation of these is, however, quite a large numerical task and we have chosen to use rates already calculated in the literature for aligned molecules and electrostatic fields. Using static field rates is indeed an approximation since the field of a 800 nm laser involves oscillations on a 2.7 fs timescale. However, the alternative of using photoionization rates averaged over an optical period will destroy the substructure in the evolution and is an even worse choice. The rates used are plotted in Fig. 4.2 as a function of both  $R$  and  $F$ .

The instant ionization rate responsible for the first ionization process ( $h \rightarrow g$ ) is calculated in Ref. [35] for  $F = 0.06$  au and  $F = 0.08$  au and interpolated to lower field strengths using the asymptotic behavior predicted by tunneling theory [37].

The second ionization process ( $g \rightarrow c$  and  $u \rightarrow c$ ) is studied in Refs. [36] and the rates are interpolated among the results published for  $F = 0.01$  au, 0.05 au, 0.05338 au and 0.08 au. Starting in the  $2p\sigma_u$  state, the rates show several peaks at large internuclear separations which, as we shall see later, induces a structure in the nuclear wave packet dynamics. This is referred to as charge resonance enhanced ionization [38, 39].

Since the rates in all the above cases are only published for molecules aligned with the external field, we exclusively study these cases, i.e.  $\theta_0 = 0$ . The gas jet used in experiments, however, has an isotropic distribution but since the coupling to the field is largest for aligned molecules this may not be such a bad an approximation after all.

## 4.4 Calculation strategy

Once the non-Hermitian Hamiltonian operator is known, the MCWP calculations can be performed. Since we use a Morse potential as the electronic energy of  $\text{H}_2$ , the vibrational wave functions are analytically known, and we assume the ground state as the initial condition,

$$K_h(R, 0) = N \cdot y^{\frac{k-1}{2}} \cdot e^{-y/2} \quad (4.32)$$

$$k = 1.2\sqrt{\mu} \quad y = k \cdot e^{(R-1.4)} \quad (4.33)$$

where  $N$  is a normalization constant.

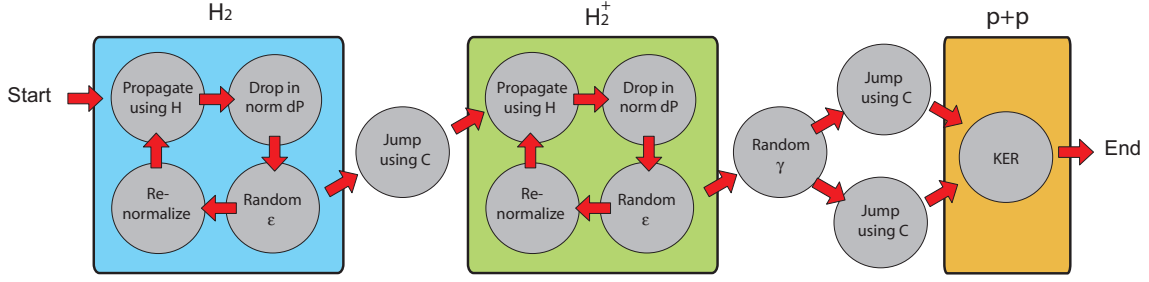


**Figure 4.3** | Overview of the calculation strategy in double ionization of H<sub>2</sub> using the MCWP approach. Each bubble corresponds to a task and the two possible paths given in the case of drawing a random number leads to a variety in the outcome of different realizations.

The field is chosen to have a Gaussian envelope and a duration of  $\tau$  (FWHM in intensity)

$$F(t) = F_{peak} \cdot \left(\frac{1}{2}\right)^{\frac{2t^2}{\tau^2}} \cdot \cos(\omega t). \quad (4.34)$$

The frequency of the light equals  $\omega$  and the peak intensity can be found using

$$I_{peak} = \frac{1}{2} c \epsilon_0 F_{peak}^2. \quad (4.35)$$

Propagation steps are calculated in close resemblance to the two-level example given earlier (see Fig. 4.3). The time evolution operator using the non-Hermitian Hamiltonian is applied to the initial state and the drop in norm is determined. Depending on a random number  $\epsilon$  we either renormalize or jump. Being in the H<sub>2</sub> system, the jump is performed by applying  $C_h$

$$|\Psi\rangle \rightarrow C_h |\Psi\rangle. \quad (4.36)$$

However, being in the H<sub>2</sub><sup>+</sup> system, two possibilities are present

$$|\Psi\rangle \rightarrow C_g |\Psi\rangle \quad \text{or} \quad |\Psi\rangle \rightarrow C_u |\Psi\rangle. \quad (4.37)$$

Which of these to choose is determined by yet another random number  $\gamma$  between zero and unity as well as the values of

$$P_g = \langle \Psi | C_g^\dagger C_g | \Psi \rangle \quad \text{and} \quad P_u = \langle \Psi | C_u^\dagger C_u | \Psi \rangle. \quad (4.38)$$

If  $\gamma < P_g / (P_g + P_u)$  a jump using  $C_g$  is the correct choice, while  $C_u$  is used if  $\gamma > P_g / (P_g + P_u)$ .

After application of both the  $C_h$  operator and either  $C_g$  or  $C_u$ , the system is purely in the doubly ionized state and further propagation of the wave function could in principle be carried out here. There is, however, no need for this since all the information concerning the kinetic energy distribution of the outgoing fragments is already present right after the second jump and an immediate projection onto energy eigenstates is performed. These are the Coulomb waves obtained by solving

$$\left(-\frac{1}{2\mu} \frac{d^2}{dR^2} + \frac{1}{R}\right) K_w(R) = EK_w(R). \quad (4.39)$$



## Calculation strategy

Even though the solutions are analytically known in terms of confluent hypergeometric functions, these are difficult to evaluate and we use instead a numerical grid solution of the equation. Using energy normalization, the density of states equals unity and the nuclear kinetic energy distribution of  $K_{final}(R)$  can be found using

$$\frac{dP}{dE} = \left| \int K_w(R) K_{final}(R) dR \right|^2. \quad (4.40)$$

By averaging over many different realizations, the correct KER spectrum is obtained and comparison with experiments can be made. However, before turning to the results, some computational aspects are discussed.

---

## Computational remarks

In the previous two chapters, it has been shown how double ionization of  $\text{H}_2$  can be simulated by propagating the nuclear wave function under the influence of a non-Hermitian Hamiltonian. Before turning to the results, we discuss in this chapter the numerical approach used for this propagation, along with ways of minimizing the computational effort.

### 5.1 Propagating the wave function

In order to propagate a wave function under the influence of an operator  $H$ , the time evolution operator is needed. In the two-level example of chapter 3, a time-independent Hamiltonian was considered, in which case the operator takes the form

$$U(t + dt, t) = \exp(-iHdt). \quad (5.1)$$

In the case of ionization processes in short intense laser pulses, the Hamiltonian is time-dependent and a very dense time grid is therefore needed to allow the application of Eq. (5.1). For each period of the electromagnetic wave we use one thousand time steps.

In order to evaluate the exponential function in the time evolution operator, one might use a Taylor expansion. However, using the approximation  $\exp(x) \approx 1 + x$  induces instability and will not conserve the norm of the wave function even when propagating using a Hermitian operator. This can be avoided by using the Crank Nicholson scheme [40] in which

$$|\Psi(t + dt)\rangle = \exp(-iHdt)|\Psi(t)\rangle \quad (5.2)$$

is approximated by solving

$$|\Psi'(t)\rangle = \left(1 - \frac{1}{2}iHdt\right)|\Psi(t)\rangle, \quad (5.3)$$

$$|\Psi'(t)\rangle = \left(1 + \frac{1}{2}iHdt\right)|\Psi(t + dt)\rangle, \quad (5.4)$$

which corresponds to propagating  $|\Psi(t)\rangle$  only half a time step forward in time, in addition to propagating  $|\Psi(t+dt)\rangle$  half a time step backwards in time. The strategy is to use Eq. (5.3) to determine  $|\Psi'(t)\rangle$  and then use this result to determine  $|\Psi(t+dt)\rangle$  in Eq. (5.4).

### 5.1.1 Finite difference grid representation

Recall the expansion of the state ket

$$|\Psi\rangle = \sum_a \int d\mathbf{R} X_a(\mathbf{R}, t) |\phi_{Ra}\rangle \otimes |R\rangle \quad (5.5)$$

$$X_a(\mathbf{R}, t) = \frac{1}{R} K_a(R, t) \frac{1}{\sqrt{4\pi}} \delta(\theta - \theta_0) \delta(\phi - \phi_0). \quad (5.6)$$

In order to perform the calculations, we chose a finite difference grid representation of the nuclear wave function  $K_a(R, t)$ . This representation contains local functions at equidistant separations  $\Delta R$  and as a consequence the potential energy becomes diagonal. The second order differential is calculated using

$$\frac{d^2}{dx^2} f|_{x_n} = \frac{f(x_{n+1}) - 2f(x_n) + f(x_{n-1}))}{\Delta x^2}, \quad (5.7)$$

where  $x_n$  are the individual grid points.

Now Eq. (5.3) is trivial to solve, while (5.4) requires the solution of a linear matrix equation. For the evolution of  $\text{H}_2$ , it involves a tri-diagonal matrix while for the singly ionized  $\text{H}_2^+$  molecule, the coupling between the  $1s\sigma_g$  and  $2p\sigma_u$  states forces the matrix to be at least six-diagonal. The equations in the latter case take the form

$$\begin{aligned} \tilde{K}_{1g}(R_n, t) = & \left[ 1 + \frac{idt}{2\mu\Delta R^2} + \frac{idt}{2} E_g(R_n) + \frac{dt}{4} |\Gamma_g(R_n)| \right] \tilde{K}_g(R_n, t+dt) \\ & - \frac{idt}{4\mu\Delta R^2} \left[ \tilde{K}_g(R_{n-1}, t+dt) + \tilde{K}_g(R_{n+1}, t+dt) \right] - \frac{idt}{2} E \cos v d_{gu} \tilde{K}_u(R_n, t+dt) \end{aligned} \quad (5.8)$$

$$\begin{aligned} \tilde{K}_{1u}(R_n, t) = & \left[ 1 + \frac{idt}{2\mu\Delta R^2} + \frac{idt}{2} E_u(R_n) + \frac{dt}{4} |\Gamma_u(R_n)| \right] \tilde{K}_u(R_n, t+dt) \\ & - \frac{idt}{4\mu\Delta R^2} \left[ \tilde{K}_u(R_{n-1}, t+dt) + \tilde{K}_u(R_{n+1}, t+dt) \right] - \frac{idt}{2} E \cos v d_{gu}^* \tilde{K}_g(R_n, t+dt). \end{aligned} \quad (5.9)$$

Existing diagonalization algorithms can relatively fast solve such problems.

## 5.2 Reducing the computational effort

When propagating the wave function in the MCWP method, several calculations turn out to be identical in each realization. Since the initial state is the same in all cases, the evolution of the wave function up until the first jump will not differ in different runs. Likewise, the evolution in the coupled  $1s\sigma_g$  and  $2p\sigma_u$  system will be identical given a specific first jump time. In order to see how this can be utilized to dramatically reduce the amount of calculations, we once again turn to the example of decay in a two level system.

### 5.2.1 Simplifications in the two-level case

Recall the two level system with decay rate  $\Gamma$  discussed in chapter 3. Using the initial wave function

$$|\phi_0\rangle = \alpha_0|g\rangle + \beta_0|e\rangle, \quad (5.10)$$

and applying the time evolution operator we obtained

$$|\tilde{\phi}_{dt}\rangle = \alpha_0|g\rangle + \beta_0|e\rangle - iE\beta_0dt|e\rangle - \frac{1}{2}\Gamma\beta_0dt|e\rangle, \quad (5.11)$$

$$\langle\tilde{\phi}_{dt}|\tilde{\phi}_{dt}\rangle \approx 1 - \Gamma\beta_0^2dt = 1 - dp. \quad (5.12)$$

The  $|\tilde{\phi}_{dt}\rangle$  state was either renormalized or projected onto the ground state but here we will do neither. Instead, the wave function is simply propagated using the non-Hermitian Hamiltonian in all the following time steps leading to coefficients with continuously falling norm,  $\tilde{N}(t)$

$$\tilde{\alpha}_{t+dt} = \tilde{\alpha}_t, \quad (5.13)$$

$$\tilde{\beta}_{t+dt} = \left[1 - iEdt - \frac{1}{2}\Gamma dt\right] \tilde{\beta}_t, \quad (5.14)$$

$$\tilde{N}(t) = |\tilde{\alpha}_t|^2 + |\tilde{\beta}_t|^2. \quad (5.15)$$

The wave function is subsequently normalized at all time steps giving a set of coefficients  $\alpha_{t+dt}$  and  $\beta_{t+dt}$ , which are physically correct in the no-jump case. Choosing only one random number  $\gamma$  in each realization, the jump time  $T$  is determined by solving

$$\gamma = \tilde{N}(T), \quad (5.16)$$

and the resulting wave functions read

$$|\phi_t\rangle = \alpha_t|g\rangle + \beta_t|e\rangle \quad t < N(T), \quad (5.17)$$

$$|\phi_t\rangle = |g\rangle \quad t \geq N(T). \quad (5.18)$$

This approach enables us to perform only a single determination of the wave function evolution in contrast to propagating from the beginning in every run. The required number of random numbers is further reduced from one in each time step to one in each realization.

Before discussing the use of the simpler method in the case of double ionization of  $\text{H}_2$ , a justification of the correctness is appropriate here. The two methods are identical if they reproduce the same jump probability  $P(t)$  in each time step. Given that a jump has already occurred, the wave function is in the ground state and both methods give zero jump probability and hence in the following, the focus will be on a system with no prior jumps.

In the original case, a random number  $\epsilon$  between zero and unity has to be smaller than the drop in norm  $dp$  in order for a jump to occur. Eq. (5.12) determines this drop in norm to equal  $\Gamma\beta_t^2dt$  giving a jump probability of

$$P_{\text{original}} = \frac{dp}{1-0} = \Gamma\beta_t^2dt. \quad (5.19)$$

The new and computationally faster method does only involve one random number  $\gamma$  and given that no jumps have appeared until now,  $\gamma$  lies in the interval between zero and  $\tilde{N}(t)$ . The jump probability thus equals

$$P_{\text{new}} = \frac{d\tilde{p}}{\tilde{N}(t) - 0} = \frac{\Gamma\tilde{\beta}_t^2 dt}{\tilde{\alpha}_t^2 + \tilde{\beta}_t^2}. \quad (5.20)$$

Renormalization is the only difference between  $(\alpha_t, \beta_t)$  and  $(\tilde{\alpha}_t, \tilde{\beta}_t)$ , so they are identical up to a prefactor  $k$ , i.e.  $\tilde{\alpha}_t = k \cdot \alpha_t$  and  $\tilde{\beta}_t = k \cdot \beta_t$ . Using this and the fact that  $\alpha_t^2 + \beta_t^2 = 1$  for all times, it is seen that

$$P_{\text{new}} = \frac{k^2 \Gamma \beta_t^2 dt}{k^2 \cdot 1} = \Gamma \beta_t^2 dt, \quad (5.21)$$

which is in perfect agreement with the original method.

In fact it is possible to reduce the amount of calculations event further and completely eliminate the random numbers. Consider the probability of obtaining a specific jump time  $T$  by solving  $\gamma = \tilde{N}(T)$ . Since the random numbers  $\gamma$  are statistically equally spaced,  $\gamma = \tilde{N}(T)$  will have more solutions in regions of large  $|d\tilde{N}(t)/dt|$ . Weighting the results at each time step with the drop in norm  $-d\tilde{N}(t)/dt$  will hence give the physical correct result. In this way, the method becomes completely deterministic and free from stochastic noise.

### 5.2.2 Simplifications in the case of H<sub>2</sub>

The simplifications of turning the stochastic MCWP technique into a deterministic method with significantly lower computationally cost apply to the case of ionization of H<sub>2</sub> as well. However, in this case several jumps are involved which slightly complicates things.

Starting with the neutral H<sub>2</sub> molecule, the full evolution in the no-jump case is determined. Denoting the norm  $\tilde{N}_h(t)$ , the jump probability equals

$$P_h(t) = -\frac{d}{dt}\tilde{N}_h(t). \quad (5.22)$$

In every time step, the jump operator  $C_h$  is applied and the wave function is renormalized and weighted with  $P_h(t)$  in order to give the starting conditions for propagation in the singly ionized H<sub>2</sub><sup>+</sup> state. This is all in close resemblance with the two-level case.

Studying the evolution in H<sub>2</sub><sup>+</sup> is, however, a bit more complicated. Here, the initial conditions are not identical in all runs and the evolution in the no-jump case must be done for every possible entering time,  $T_1$ . The drop in norm now determines the conditional probability of a second jump at time  $T_2$  given an initial jump at time  $T_1$

$$P_{gu}(T_2 | T_1) = -\frac{d}{dt}(\tilde{N}_g(T_2) + \tilde{N}_u(T_2)). \quad (5.23)$$

In order to do the second jump, either  $C_g$  or  $C_u$  is applied and also the choice of which one is done deterministically. Weighting the final results with

$$P_g(g | \{T_1, T_2\}) = -\frac{\langle \Psi | C_g^\dagger C_g | \Psi \rangle}{\langle \Psi | C_g^\dagger C_g + C_u^\dagger C_u | \Psi \rangle}, \quad (5.24)$$

$$P_u(u | \{T_1, T_2\}) = -\frac{\langle \Psi | C_u^\dagger C_u | \Psi \rangle}{\langle \Psi | C_g^\dagger C_g + C_u^\dagger C_u | \Psi \rangle}, \quad (5.25)$$

takes care of this. The projections are calculated for all times, generating input to the doubly ionized  $\text{H}_2^{++}$  system.

In the doubly ionized state, the KER is determined for all values of the two jump times  $T_1$  and  $T_2$ . Following the above discussion, the final result is obtained by doing the weighted summation

$$\text{KER}_{\text{tot}} = \sum_{T_1, T_2} P_h(T_1) P_{gu}(T_2|T_1) \left[ \sum_{a=g,u} P_a(a|\{T_1, T_2\}) \text{KER}_a(T_1, T_2) \right]. \quad (5.26)$$

Since a very dense time grid is used, determining all possible  $\text{KER}_g(T_1, T_2)$  and  $\text{KER}_u(T_1, T_2)$  is computationally expensive and the initial jump is assumed to occur only at the field extrema and the second jump is only allowed in every tenth time step, i.e. 100 times in every laser period. In this way, the full propagation of the molecule exposed to an intense laser pulse of 40 fs duration reduces to one full propagation in the  $\text{H}_2$  system and approximately 30 propagations in the  $\text{H}_2^+$  system with different start times. After completing the  $\text{H}_2$  evolution, the remaining calculation can be made in parallel and the total computation time is on the order of 2-4 hours.

# Results

In this chapter, results of the MCWP calculations on  $H_2$  as well as  $D_2$  are presented. Since the separation of timescales has been a critical point in the derivation, the agreement with experiments is expected to be best for heavy nuclei and we therefore first consider  $D_2$ . Hereafter, results for  $H_2$  are presented as well. The pulses used in both cases have a wave length of 800 nm, a peak intensity of  $1.0 \cdot 10^{14} \text{W/cm}^2$  and a pulse duration (FWHM) of 40 fs. At the end of the chapter, a short discussion of results using other pulse parameters is given.

## 6.1 Nuclear dynamics of the neutral molecule

Starting in the electronic and nuclear ground state of  $D_2$ , the evolution of the neutral molecule is the first to be calculated. The results are given in Fig. 6.1 using the peak of the pulse as origin of the time axis. Panel (a) gives the probability density  $|\tilde{K}_h(R, t)|^2$  in the electronic state  $(1s\sigma_g)^2$  as a function of both internuclear separation and time. Integrating over all possible separations, the norm is obtained and plotted in panel (b). As seen from the norm, only approximately 0.15% of the molecules undergo ionization, which together with the initial condition results in almost no changes in the probability distribution of panel (a) as a function of time. However, dynamics do indeed appear as seen

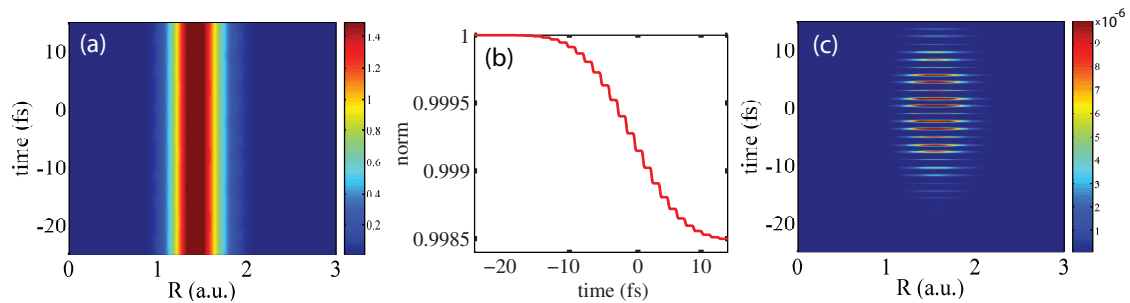


**Figure 6.1** | Results for the first ionization step in  $D_2$ . Panel (a) shows  $|\tilde{K}_h(R, t)|^2$ , panel (b) shows  $\int |\tilde{K}_h(R, t)|^2 dR$  and panel (c) shows the population density transferred to the  $D_2^+$  system.

from panel (c) which shows the probability density entering the singly ionized state. More precisely,  $C_h|\Psi\rangle$  have been calculated, normalized and weighted by the jump probability  $P_h(t)$  for all times and  $|K_g(R, t)|^2$  is plotted. Population is transferred mostly at the extrema of the external field with maximum at the peak of the pulse just as expected. To the careful eye it is seen that the density is shifted a little towards larger internuclear distances reflecting the tendency in the rate  $\Gamma_h$  as a function of this parameter, see Fig. 4.2.

## 6.2 Dynamics in the singly ionized molecule

Even though the density distribution entering the singly ionized state is shifted compared to the ground state of  $D_2$ , it is still centered at relatively small internuclear distances ( $\sim 1.5$  au). Since the equilibrium distance in  $D_2^+$  is 2.0 au this induces nuclear dynamics as seen from Fig. 6.2. Panel (a) shows  $|\tilde{K}_g(R, t)|^2$  under the assumption that the first ionization occurs 7.3 fs before the peak of the pulse, and  $|\tilde{K}_u(R, t)|^2$  is plotted in panel (b) using the same initial conditions. The characteristic vibrational timescale of 24 fs in the  $1s\sigma_g$  state is reflected in the nuclear dynamics of panel (a) and the coupling to the  $2p\sigma_u$  state transfers population up and down. The  $2p\sigma_u$  state is dissociative and the wave function spreads out in panel (b). Using the slope of an imaginary line from the lower left corner to the upper right corner as a classical estimation of the kinetic energy, this is on the order of 1.5 eV.

Together with the dissociation a very peaked structure is seen in panel (b). In order to see this structure more clearly, a zoom is given in panel (c) showing that there are two peaks in every half period of the light ( $\tau = 2.7$  fs). This structure can be understood by examining the difference in order of the  $1s\sigma_g$ - $2p\sigma_u$  coupling and the ionization process. The  $1s\sigma_g$ - $2p\sigma_u$  coupling is a low order process and the channel opens at relatively low field strengths. Population is transferred from the  $1s\sigma_g$  state until the field is close to maximum, opening the ionization channel and depleting the  $2p\sigma_u$  state. After the field extrema, the ionization channel closes again and the coupling to the  $1s\sigma_g$  state once again leads to population growth. When also this channel closes, the norm in the  $2p\sigma_u$  state stays almost constant and dissociation just gives the illusion that the norm drops. Hence the two-peaked structure.

In addition to modulation as a function of time,  $|\tilde{K}_u(R, t)|^2$  shows modulation as a function of internuclear separation. This modulation is mainly due to the peaks in the ionization rate  $\Gamma_u(R)$  at large distances referred to as charge resonance enhanced ionization, see Fig 4.2. Even though the evolution shown is calculated in the no-jump case, the dynamics are still affected by the ionization rate, just as seen in the two-level example where the population in the ground state raises despite the detection of no transitions. This effect is referred to as the Lochfrass effect [41]. In regions of high ionization rate, the probability density is lowered, while it is raised in regions of high ionization rate.

### 6.2.1 The second jump

The modulation in population density is also seen in the states entering the doubly ionized space. Panel (d) and (e) of Fig. 6.2 show the probability density right after the second jump from  $1s\sigma_g$  and  $2p\sigma_u$  respectively. In the  $2p\sigma_u$  case, the structure of the rates is seen and the maximum transfer is observed 10 fs after the peak of the pulse since the wave function at this time is more dense in the regions of high rates than earlier in the



## Jump probabilities

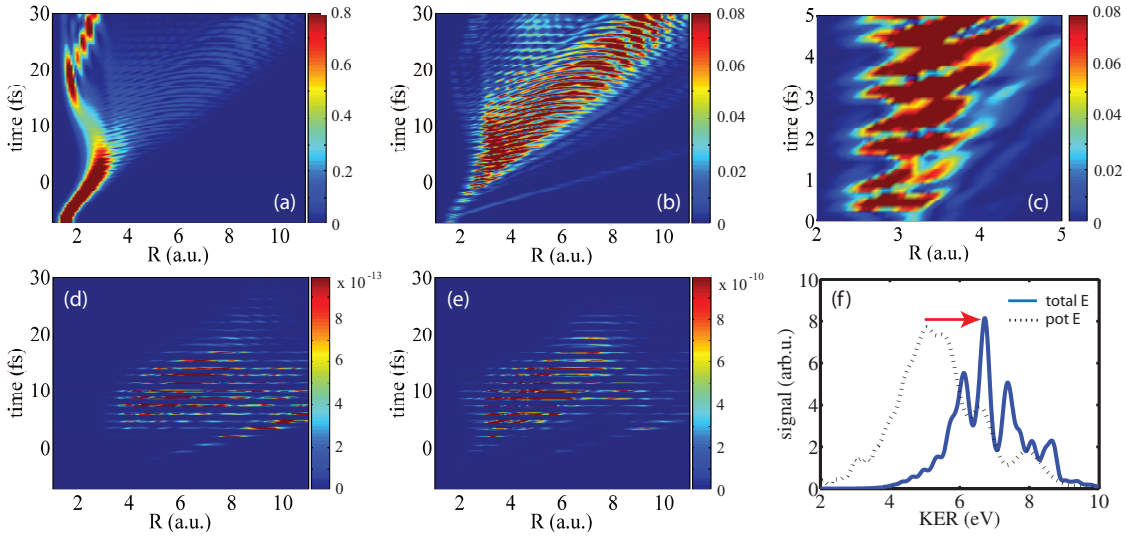


**Figure 6.2** | Results concerning the second ionization step in  $D_2$ . Panel (a) and (b) shows  $|\tilde{K}_g(R, t)|^2$  and  $|\tilde{K}_u(R, t)|^2$  respectively, with panel (c) being a zoom of the latter. Panel (d) and (e) show the population density leaving the two states resulting in the energy distribution of panel (f).

pulse. Turning to the  $1s\sigma_g$  case almost the same picture is observed. This is despite the fact that the wave function in the  $1s\sigma_g$  state has almost no weight at these large internuclear separations. The population transferred accordingly corresponds to molecules first dissociating on the  $2p\sigma_u$  potential curve and later coupled back to the  $1s\sigma_g$  system for the later ionization. Due to this more complicated route involving two transitions in the singly ionized space, the amount of population transferred in this way is down by a factor of 1000 compared to the amount transferred directly from the  $2p\sigma_u$  state (see colorbar). In the following, ionization from the  $1s\sigma_g$  state is hence completely neglected. Both couplings were included in the theoretical discussion since transitions from various states may turn out to be very important in other diatomic molecules.

Having determined the probability density right after the second jump allows the projection onto Coulomb states in order to find the KER. Panel (f) shows the result summed over all possible second jump times but restricted to a first jump at time 7.3 fs prior to the peak. The spectrum is centered at 6.5 eV, is approximately 4 eV wide and shows a sharply peaked structure. To understand this structure, the potential energy of the two nuclei at the time of the second ionization is also plotted. Peaking at only 5 eV, the kinetic energy obtained in the dissociation process is seen to be on the order of 1.5 eV in full agreement with the estimate from panel (b) and recent non-Born-Oppenheimer calculations [20]. In addition to the overall shift, the dissociation energy also adds structure to the resulting spectrum and this is the main reason for the peaks.

### 6.2.2 Jump probabilities

Before turning to the final result obtained by summation over all possible jump times, the weights of the individual contributions are considered. The ionization rate peaks at the maximum of the field and one may expect two ionizations close to the center to give the largest contribution. However, the rate raises significantly at large internuclear separations and sufficient time to dissociate is important, leaving a first jump at 7.3 fs prior to the

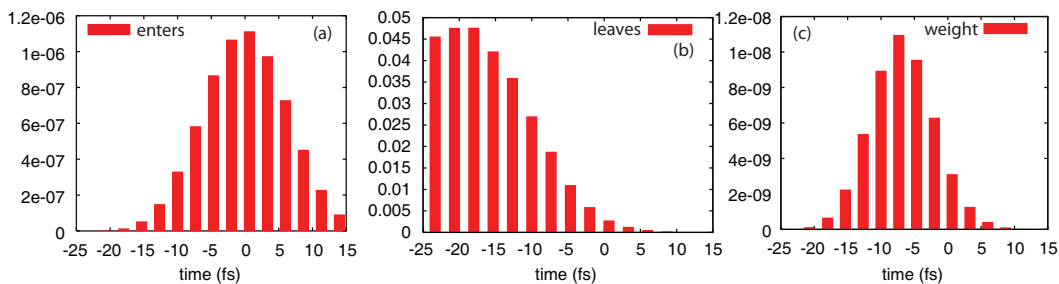


**Figure 6.3** | The probability to enter and leave the singly ionized state of  $D_2$ . A product of the two gives the weight of the individual contributions.

peak and a second jump at 10.2 fs after the peak as the greatest contributor.

Fig. 6.3 shows how the result of  $-7.3$  fs as the most important first jump time comes about. Panel (a) indicates the probability of the first ionization  $P_h(t)$  centered around the origin as expected. Panel (b) on the other hand gives the probability of a second ionization given a first ionization at time  $T_1$

$$\int_{T_1}^{\infty} P_{gu}(t|T_1)dt, \quad (6.1)$$

and shows maximum at 20 fs prior to the peak, making the wave function reach the region of high rates at maximum intensity. Multiplying the two results shows the weight peaking at  $-7.3$  fs in panel (c). The most important second ionization time at 10.2 fs is easily found by examination of panel (e) in Fig. 6.2.

### 6.3 Comparison with experiments

Even though the most important contribution is discussed in the previous subsection, a summation over all the possible contributions is needed in order to compare with experiments. Fig. 6.4 shows the total result and experimental data published in [21] in the case of both  $D_2$  and  $H_2$ .

A very good agreement between theory and experiments is observed in the  $D_2$  case of panel (a). The signal rises from 2 to 6 eV with nearly perfect slope and reveals rich structure, peaking at the correct positions from 6 to 9 eV. It is the evolution on the coupled  $1s\sigma_g-2p\sigma_u$  curves which gives this structure, and the approximately one quarter of kinetic energy and three quarters of potential energy which give the correct width and center energy of the overall spectrum.

The two-surface model [21] and the ab initio calculations [20] both mentioned in chapter 2 also reproduce the major part of the spectrum very well. However, they both lack the peak at 9 eV. By performing calculations leaving out the  $R$ -dependence of the ionization rates in the  $D_2 \rightarrow D_2^+$  step, a similar suppression of the 9 eV peak is found. This analysis supports the MCWP approach which properly includes the mapping of the wave function with an  $R$ -dependent ionization rate throughout the dynamics.

Turning to the result for  $H_2$  in panel (b), the agreement with experimental data is not quite as impressive as for  $D_2$ . However, the center of the spectrum at 5.5 eV is correctly reproduced and so is the width of  $\sim 5$  eV. The Born-Oppenheimer separation is expected to be slightly less applicable due to the lighter nuclei. However, the deviation may be a result of other approximations as well. By assuming that all molecules are aligned

## Using other pulse parameters

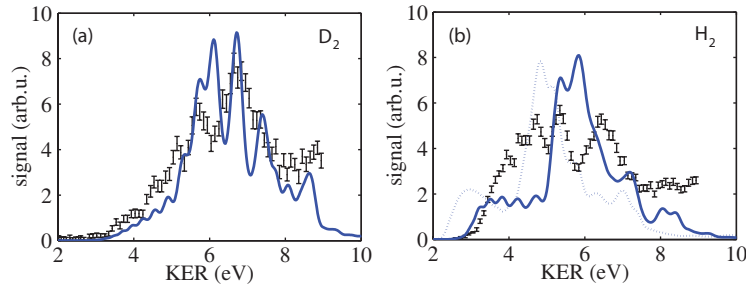


**Figure 6.4** | Numerical results (line) and experimental data (dots) [21] in the case of D<sub>2</sub> and H<sub>2</sub> exposed to laser pulses of 800 nm, 40 fs and  $1.0 \cdot 10^{14}$  W/cm<sup>2</sup>. In panel (b) also the result using an intensity of  $0.6 \cdot 10^{14}$  W/cm<sup>2</sup> is given (dotted line).

along the field polarization and experience the same peak intensity, we only account for molecules with maximum coupling to the field. Lowering the intensity shifts the position of the individual peaks down in energy and this has to be accounted for if perfect agreement is to be expected. To illustrate this effect, the dotted line in panel (b) shows the result for a peak intensity lowered by 40%.

## 6.4 Using other pulse parameters

The above discussion concerned pulses characterized by a wavelength of 800 nm, a pulse duration of 40 fs (FWHM) and a peak intensity of  $1.0 \cdot 10^{14}$  W/cm<sup>2</sup>. Lowering the intensity enhance the effect of difference in order of the  $1s\sigma_g$ - $2p\sigma_u$  coupling and the ionization process and hence leads to more dissociation prior to ionization. In this way, the spectrum is shifted towards lower energies as is also observed experimentally [22].

Using pulses of longer duration in a similar way leads to more dissociation and therefore a lower kinetic energy release. The MCWP technique has in principle no upper limit to the pulse duration. However, reaching regions of almost constant intensity will reduce the complexity of the problem and hence allow for simpler models to succeed as well. In a similar way, short pulse durations on the time scale of nuclear motion are not as interesting in a MCWP description, since the ability to account for dynamics under the pulse is irrelevant.

Turning to other wave lengths, calculations have been made using 395 nm light giving reasonable results, however, the model is assumed to be best in the long wavelength regime since static field rates are used.

Finally, it should be mentioned that even though the presented theory concerns H<sub>2</sub> and D<sub>2</sub>, it is just as applicable to describe ionization of ionbeams containing H<sub>2</sub><sup>+</sup> and D<sub>2</sub><sup>+</sup>. The first ionization step is simply removed from the calculations. A few simulations have been made in order to reproduce the data of Ref. [23], however, finding the correct initial condition has shown to be rather difficult and is a work in progress.

---

# Conclusion

In studying the Coulomb explosion of  $H_2$  and  $D_2$  exposed to short intense laser pulses, the MCWP technique has proven to reproduce the KER spectrum of the protons quite well. With the correct peak positions, broadness, and for deuterium even the correct substructure of the spectrum, the model most certainly succeeds in the attempt to describe nuclear dynamics in double ionization processes. Using a deterministic version of the stochastic jump model, both ionizations can be handled on an equal footing and the calculations reduce to propagating one or two level Schrödinger equations using a non-Hermitian Hamiltonian. As long as the static field rates are known, the MCWP technique can be generalized to include several more bound states and as many jumps as desired. In this way, it may serve as an important tool for the future understanding of strong field processes and molecular dynamics.

## 7.1 Outlook

Generalization of the MCWP technique to other and larger systems is an obvious and interesting challenge. This includes both diatomic molecules such as  $N_2$  and  $O_2$  with more electrons and hence possibly the need for more jumps but also molecules with more than two nuclei. In describing polyatomic molecules, simple models are indeed desired and the MCWP technique is here an obvious candidate.

Before turning to larger systems, several improvement in the present model can be made as well. In studying double ionization of  $H_2$ , the ionization rates are very critical, especially at the rising of the pulse where the dissociation process is initiated. Since the rates used in this report are interpolations of only five different field strengths, this is an obvious place for improvements. In addition, averaging over different orientations and spacial focus effects are important if full agreement with experiments is to be obtained.

With these improvements made, other less critical approximations can likewise be improved. It would be interesting to see if including extra electronic bound states will change the results noticeably or to try and add rescattering of the electrons in the model.

Studying the distinguishability of ionization from  $1s\sigma_g$  and  $2p\sigma_u$  could be interesting as well. In writing up Eqs. (4.30) and (4.31), we assumed the jumps to be distinguishable. However, if this is not the case, a linear combination of the two should be used which will

## Outlook

lead to interference terms. Handling the evolution in the  $1s\sigma_g$  and  $2p\sigma_u$  systems correctly and studying their relative phases may provide a theoretical explanation of the recent experiments on electron location in ionization and dissociation of  $D_2$  [11].

Control over larger molecules such as selective bond breaking in the water isotopologue HOD could be another future application. Several schemes for such control have been proposed [42]. However, all of these neglect the ionization channel. This is very critical since often, the intensities used in these control schemes are very high and hence most probably will lead to ionization. We hope to use the MCWP technique in order to include this channel and improve the future description of this kind of control over chemical processes.



---

# Bibliography

- [1] H. A. Leth, L. B. Madsen, and J. F. McCann, *Phys. Rev. A* **76**, 033414 (2007).
- [2] H. A. Leth, L. B. Madsen, and K. Mølmer, submitted for publication in *Phys. Rev. Lett.* (2009).
- [3] M. Göppert-Mayer, *Annalen der Physik* **401**, 273 (1931).
- [4] W. Kaiser and C. G. B. Garrett, *Phys. Rev. Lett.* **7**, 229 (1961).
- [5] J. L. Hall, E. J. Robinson, and L. M. Branscomb, *Phys. Rev. Lett.* **14**, 1013 (1965).
- [6] P. Agostini, F. Fabre, G. Mainfray, G. Petite, and N. K. Rahman, *Phys. Rev. Lett.* **42**, 1127 (1979).
- [7] B. W. Shore and P. L. Knight, *J. Phys. B* **20**, 413 (1987).
- [8] A. S. Alnaser, B. Ulrich, X. M. Tong, I. V. Litvinyuk, C. M. Maharjan, P. Ranitovic, T. Osipov, R. Ali, S. Ghimire, Z. Chang, et al., *Phys. Rev. A* **72**, 030702 (2005).
- [9] T. Ergler, A. Rudenko, B. Feuerstein, K. Zrost, C. D. Schröter, R. Moshhammer, and J. Ullrich, *Phys. Rev. Lett.* **95**, 093001 (2005).
- [10] T. Ergler, A. Rudenko, B. Feuerstein, K. Zrost, C. D. Schröter, R. Moshhammer, and J. Ullrich, *Phys. Rev. Lett.* **97**, 193001 (2006).
- [11] M. F. Kling, C. Siedschlag, A. J. Verhoef, J. I. Khan, M. Schultze, T. Uphues, Y. Ni, M. Uiberacker, M. Drescher, F. Krausz, et al., *Science* **312**, 246 (2006).
- [12] K. Burnett, V. C. Reed, and P. L. Knight, *J. Phys. B* **26**, 561 (1993).
- [13] T. Brabec and F. Krausz, *Rev. Mod. Phys.* **72**, 545 (2000).
- [14] J. H. Posthumus, *Rep. Prog. Phys.* **67**, 623 (2004).
- [15] F. Krausz and M. Ivanov, *Rev. Mod. Phys.* **81**, 163 (2009).

## Bibliography

- [16] J. Ullrich, R. Moshhammer, R. Döner, O. Jagutzki, V. Mergel, H. Schmidt-Böcking, and L. Spielberger, *J. Phys. B* **30**, 2917 (1997).
- [17] R. Dörner, V. Mergel, O. Jagutzki, L. Spielberger, J. Ullrich, R. Moshhammer, and H. Schmidt-Böcking, *Phys. Rep.* **330**, 95 (2000).
- [18] M. Sindelka and N. Moiseyev, *J. Phys. Chem. A* **110**, 5561 (2006).
- [19] M. Førre and H. Bachau, *Phys. Rev. A* **77**, 053415 (2008).
- [20] M. Vafaei, *Phys. Rev. A* **78**, 023410 (2008).
- [21] A. Staudte, D. Pavičić, S. Chelkowski, D. Zeidler, M. Meckel, H. Niikura, M. Schöffler, S. Schössler, B. Ulrich, P. P. Rajeev, et al., *Phys. Rev. Lett.* **98**, 073003 (2007).
- [22] S. Chelkowski, A. D. Bandrauk, A. Staudte, and P. B. Corkum, *Phys. Rev. A* **76**, 013405 (2007).
- [23] B. D. Esry, A. M. Sayler, P. Q. Wang, K. D. Carnes, and I. Ben-Itzhak, *Phys. Rev. Lett.* **97**, 013003 (2006).
- [24] I. Ben-Itzhak, A. M. Sayler, P. Q. Wang, J. McKenna, B. Gaire, N. G. Johnson, M. Leonard, E. Parke, K. D. Carnes, F. Anis, et al., *J. Phys: Conference Series* **88**, 012046 (2007).
- [25] D. S. Murphy, J. McKenna, C. R. Calvert, W. A. Bryan, E. M. L. English, J. Wood, I. C. E. Turcu, W. R. Newell, I. D. Williams, and J. F. McCann, *J. Phys. B* **40**, S359 (2007).
- [26] J. Dalibard, Y. Castin, and K. Mølmer, *Phys. Rev. Lett.* **68**, 580 (1992).
- [27] H. J. Carmichael, *An Open Systems Approach to Quantum Optics* (Springer-Verlag, Berlin Heidelberg, 1993).
- [28] K. Mølmer and Y. Castin, *Quant. Semiclass. Opt* **8**, 49 (1996).
- [29] K. Mølmer, Y. Castin, and J. Dalibard, *J. Opt. Soc. Am. B* **10**, 524 (1993).
- [30] L. B. Madsen and D. Dimitrovski, *Phys. Rev. A* **78**, 023403 (2008).
- [31] D. Dimitrovski and L. B. Madsen, *Phys. Rev. A* **78**, 043424 (2008).
- [32] P. J. Lindstrom and W. G. Mallard, *Nist chemistry webbook, nist standard reference database number 69*, <http://webbook.nist.gov/chemistry/>.
- [33] L.-Y. Peng, Ph.D. thesis, The Queen's University Belfast (2005).
- [34] F. Anis, T. Cackowski, and B. D. Esry, *J. Phys. B* **42**, 091001 (2009).
- [35] A. Saenz, *Phys. Rev. A* **66**, 063408 (2002).
- [36] M. Plummer and J. F. McCann, *J. Phys. B* **29**, 4625 (1996).
- [37] X. M. Tong, Z. X. Zhao, and C. D. Lin, *Phys. Rev. A* **66**, 033402 (2002).

## Bibliography

- [38] A. D. Bandrauk and J. Ruel, Phys. Rev. A **59**, 2153 (1999).
- [39] A. D. Bandrauk and H. Z. Lu, Phys. Rev. A **62**, 053406 (2000).
- [40] W. H. Press, S. A. Teukolsky, W. T. Vetterling, and B. P. Flannery, *Numerical Recipes* (Cambridge University Press, Cambridge, England, 1992).
- [41] E. Goll, G. Wunner, and A. Saenz, Phys. Rev. Lett. **97**, 103003 (2006).
- [42] A. K. Tiwari, K. B. Møller, and N. E. Henriksen, Phys. Rev. A **78**, 065402 (2008).